Computer Studies of D-Ion Induced Atomic Displacement Rate and Deuterium Reemission Rate of Nickel with Absorbed Deuteriums

AUTHOR(S):

SHIN, Kazuo; OGAWA, Hirohumi

Computer Studies of D^+-Ion Induced Atomic Displacement Rate and Deuterium Reemission Rate of Nickel with Absorbed Deuteriums

by

Kazuo SHIN and Hirohumi OGAWA*

(Received December 24, 1991)

Abstract

The D^+ ion induced atomic displacement rate and reemission of energetic deuterons were analyzed by BCA-model calculations for nickel metal having absorbed deuterons on its surface, or containing absorbed deuterons in the bulk (NiD mixture). The results were compared with those for the pure nickel metal and the nickel oxide.

The NiD mixture showed a large change in the D^+ projected range and the Ni atom displacement rate because of the influence of contained deuterons. The displacement rate of D atoms in the NiD was very large. The number of emitted D atoms from the D adsorbate layer on the Ni metal surface was about 30% at maximum of the total number of reflected D atoms.

I. Introduction

First wall and structure materials in fusion reactors are irradiated by high fluence of high energy fusion neutrons. The recoil of target atoms by neutrons initiates a displacement cascade in the materials, which introduces neutron damage in the materials. First wall and divertor plates are also exposed to the bombardment of hydrogen isotopes and alpha particles from plasma. The implanted hydrogen isotopes mostly stay near the surface of the metal and then diffuse into the bulk. The existence of large amounts of hydrogen isotopes in materials may have an influence on the sputtering yield, displacement rate of atoms and hydrogen ion reflection rate of the materials.

The simulation of collision cascades in solids has been made by the molecular dynamics method/1/ or the Monte Carlo method./2, 3/ The molecular dynamics method solves the problem as a multibody problem, hence needs much more computing time than the Monte Carlo method. This restricts the application of the molecular dynamics method to lower energy cascade calculations. The Monte Carlo method is a method applicable to the simula-

* Department of Nuclear Engineering, Kyoto University

tion of collision cascades initiated by higher energy ions.

There are already several Monte Carlo codes/2–4/ based on the binary collision approximation (BCA model), like MARLOWE/2/ and TRIM./3/ They have been applied to the calculation of the sputtering and displacement rate for monolayered materials. Yamamura/4/ first simulated, by the BCA model, an Ar induced sputtering rate of W which absorbed N atoms on its surface.

In this work, a BCA model code is applied to estimate the deuteron–ion–induced sputtering and displacement of nickel metal which absorbs deuteriums. The reflection of deuteriums by nickel which chemisorbs deuteriums on its surface is also estimated by the code. Similar calculations are also made for pure Ni and nickel oxide (NiO), and the influence of deuterons existing in the metal to the above parameters are tested.

II. Calculational Model

The process of collision cascade simulation was the Monte Carlo method based on the binary collision approximation (BCA model). A code developed by Kido/5/ was slightly modified and used here. The Monte Carlo calculation used was straight forward with no biasing technique except for TRIM/3/–like path stretching which was used at higher energies.

Targets assumed in the code were made up of 5 sublayers at maximum, each of which was composed of up to 5 elements and had a homogeneous amorphous structure. The lattice constant was decided by the nominal cell model, i. e., $\lambda = n^{-1/3}$, with n being the atomic density.

The calculation of scattering paramenters in an elastic collision was carried out approximately by the TRIM technique/3/at high energies, i. e., $\varepsilon > 0.2$, where ε is the nondimensional reduced energy. But the calculations were made more rigorously at low energies ($\varepsilon \leqq 0.2$) by performing the time integration as in the MARLOWE code./2/ The interatomic potential was selected from the Molier approximation/6/ for Thomas–Fermi potential or Kr –C potential/7/ with a Firsov screening parameter,/8/ depending on the energy of the colliding atom.

The energy loss ΔE_e by the inelastic collision was computed independently from the elastic collision as follows : At higher energies, i. e., $\varepsilon > 0.2$,

$$\Delta E_e = LNS_e(E), \tag{1}$$

where L = distance between two subsequent collisions,

$S_e(E)$ = electron stopping cross section.

The collision distance L was set equal to the lattce constant. The distance, however, was stretched at higher energies by the TRIM technique to avoid simulating very forward

scattering whch does not produce any displacement of atoms.

The electrical stopping cross sections were computed by the Anderson & Ziegler formula/9/ for H, the ziegler formula/10/ for He, the Lindhard Scharff formula/11/ and the modified Bethe–Bloch formula/12/ for heavy ions. The above formulae were used with the Varelas & Biersack interpolation method/13/ which combined the formulae for the higher and lower energy regions to estimate the cross section in the intermediate energy range.

In the simulation of the collision cascade, each atom was traced until its energy dropped below a cutoff energy E_c. The cutoff energy was set as $E_c=5$eV throughout the whole calculation process.

III. Results of Simulations

The displacement and sputtering of Ni atoms was analyzed by using four forms of nickel i. e., pure nickel metal (Ni), nickel metal with adsorbed deuteriums on its surface (Ni with D adsorbate layer), Nickel metal containing absorbed deuterons uniformly in the bulk (NiD mixture) and nickel oxide (NiO). The reflection rate of energetic deuterons by these metals was also computed.

Before these calculations, the binding energy of the displaced atom was varied and the impact of the variation to calculated results was tested.

(1) Selection of Binding Energy

The displacement energy E_d is defined such that the recoiled atom receiving more energy than E_d in an atomic collision is displaced from the original location. As is shown in Fig. 1, the recoiled atom joins the cascade with the energy $T-E_b$, where $T(\geqq E_d)$ is the energy given to the atom in the collision, and $E_d(\leqq E_d)$ is the binding energy of the atom to the lattice. The BCA calculation assumes collisions between two quasifree atoms and neglects the binding effect of the atom to the lattice. The binding effect is taken into consideration only in an approximate manner by the selection of the different E_b value.

Here we assume two cases, i. e., $E_b=E_d$(Model 1) and $E_b=E_d/2$(Model 2). The displacement energy of Ni is fixed at $E_d=20$ eV following other similar calculations. However, up to the depth of 10Å, $E_d=E_s$ is used, where E_s is the sublimation energy of the Ni metal and is 4.4eV. The same displacement energy is also assumed for O atoms. However, the energy is set at zero for absorbed deuteriums, considering the very weak binding of deuteriums in the metal.

As an example for the test of the binding energy model, D^+, Ar^+ ions are injected onto the Ni metal, and the displacement rate of Ni is calculated assuming the above two binding energies.

Table I shows the results of the calculations for the incidence of 1 or 10 keV D^+ ions.

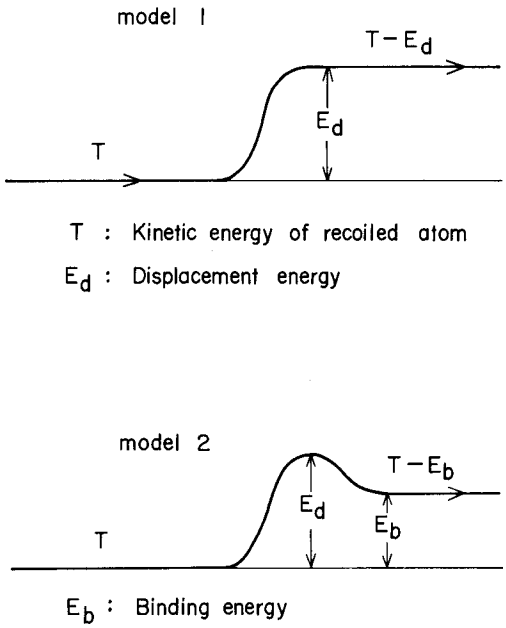

Fig. 1 Atomic displacement with two different binding energies.

Table I Number of Displacement Events of Ni Atom in Ni Target Induced by D^+ Ion Injection.

D^+ Energy (keV)	Amount of Ni Displacement ($1/D^+$ Ion)	
	Model 1	Model 2
1	4.8	5.3
10	20.7	22.0

The kinetic energy of recoiled Ni atoms increases by 10 eV, since E_b varies from E_d to $E_d/2$. This may increase the possibility of generating new displacement by these recoiled Ni atoms. However an actual displacement cascade is not generated in Ni by 10 keV D^+ ions; most Ni displacement is caused by primary D^+ ions. So the increasing rate in the amount of displacement by Model 2 is not large (10%).

Similar results are listed in Table II for the Ar^+ ion incidence. The energy of Ar^+ ions is 1 or 10 keV. At the incident energy of 1 keV, the amount of displacement increases by about 10% in the Model 2 calculation. However the increasing rate is about double in the 10 keV case, where the collision cascade occurs and a greater number of Ni atoms are displaced by recoiled Ni atoms in the Model 2 calculation.

A similar tendency (~20% increase) is also seen in the results of Table III for the

Table II Number of Displacement Events of Ni Atom in Ni Target Induced by Ar Ion Injection.

Ar Energy (keV)	Amount of Ni Displacement (1/Ar Ion)	
	Model 1	Model 2
1	64	71
10	283	336

Table III Number of Displacement Events of Ni Atom in Ni Target Induced by Ni Ion Injection.

Ni Energy (keV)	Amount of Ni Displacement (1/Ni Ion)	
	Model 1	Model 2
10	300	364
100	1880	2319

Ni^+ incidence case, where both the mass number of projectiles and the incident energy are higher.

In conclusion, the change in the E_b value varies the calculated results by about 20% depending on the incident ion and energy.

(2) Sputtering Yield of Ni

To test the accuracy of the present code calculation, the sputtering yield of Ni is calculated for Ar^+ and Ni^+ ion incidence, and the results are compared with the experimental data of Ref. 14.

Figure 2 shows the results for the Ar^+ incidence. The calculation was made with the incident energies, 0.1, 1 and 10 keV using the above binding energy modles 1 and 2. Both binding energy models gave very similar results. The calculated results agree very well with the experimental data at 0.1 and 1 keV. However, slight underestimation is observed at 10 keV. This is caused by the lack of the thermal spike effect in the BCA model. The effect gets more important in cases where the incident energy is higher. However the effect is a multibodied one and is not taken into consideration in the BCA cascade calculation.

Figure 3 shows corresponding results for the Ni^+ incidence. The agreement between this calculation and the experimental values seems good at 10 keV. But the slight underestimation in the calculation is observable for the data at 100 keV. The reason for this disagreement is again the effect of the thermal spike.

Except for the slight underestimation at higher energies, the Ni sputtering yield data were well reproduced by the calculation.

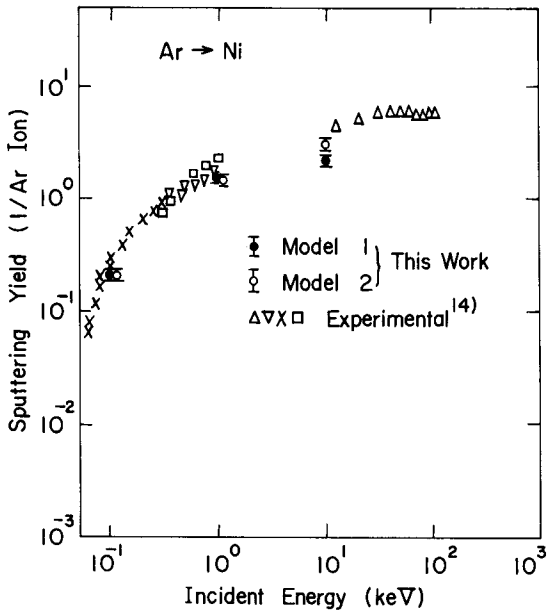

Fig. 2 Sputtering yield of Ni bombarded by Ar ions.

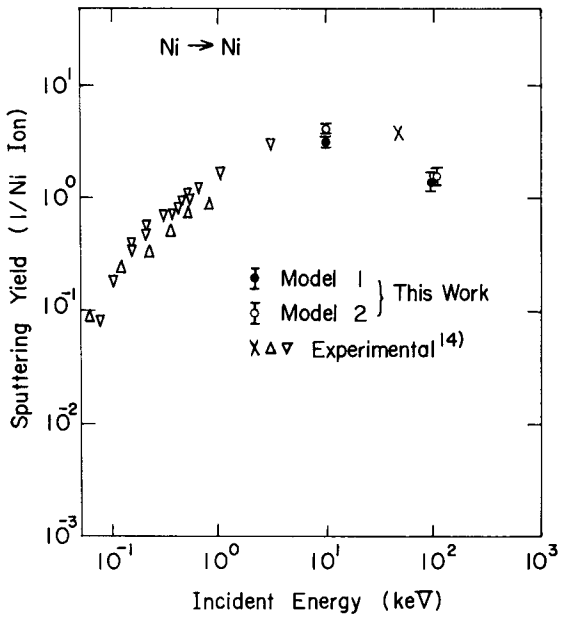

Fig. 3 Sputtering yield of Ni bombarded by self ions.

(3) Injection of D^+ into Nickel Metals

(a) Projected Range of D in pure Ni

The projected range of 200 keV D^+ in Ni was calculated and compared with the measured data. Calculation was made assuming the Model 1 binding energy.

The experiment was performed by the nuclear reaction method. The D^+ ions were injected into a Ni specimen at 200 keV energy by a Cockcroft–Walton accelerator at liquid nitrogen temperature. Then the specimen was irradiated by a $^3He^+$ probing beam to detect D in the specimen by measuring protons from the nuclear reaction $^3He(D, \alpha)p$. The proton spectrum was then converted to the D depth profile in the Ni specimen using ^3He energy dependent cross sections of the reaction.

Figure 4 shows the results obtained. Experimental data in the figure exhibits rather broader distribution, since the broadening owing to the finite resolution of the measuring system was not removed. The calculated projected range shows slight broadening caused by the straggling and multiple collision effect of ^3He and p.

The peak depths of the two range distributions in the figure differ from each other. The electron stopping cross section used in the calculation may be slightly underestimated.

(b) NiD, NiO and Ni with D Adsorbate Layer

Calculations were made for cases where D^+ ions were injected into the Ni metal, the NiD mixture, the NiO and the Ni with D adsorbate layer.

The atomic density of the assumed Ni metal was 9.08×10^{22} atoms/cm^3. For the NiD

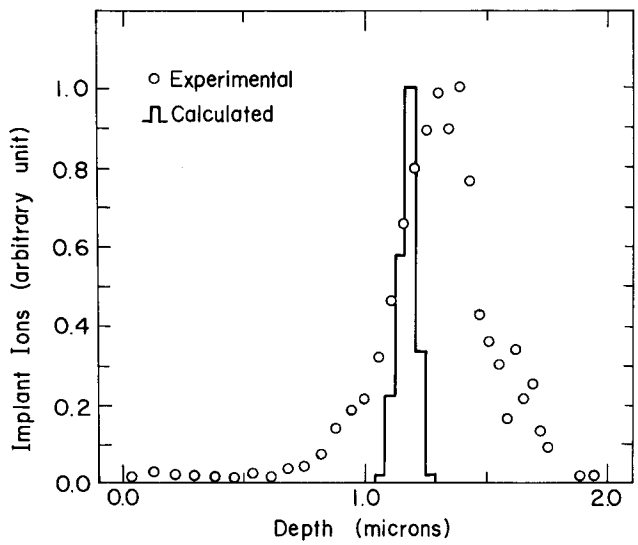

Fig. 4 Comparion of measured and calculated projected range distributions of 200-keV D^+ ions implanted into Ni.

mixture, the same atomic density of Ni atoms was assumed and the same number of D atoms were uniformly distributed in the metal. The atomic density of Ni and O atoms in the NiO specimen was 1.12×10^{23} atoms/cm^3. For the Ni with D adsorbate layer, a D layer of 5 Å was assumed as the adsorbate layer on the surface of pure Ni metal. The atomic density of D atoms in the adsorbate layer was the same as that of Ni in the Ni metal. The 5 -Å wide layer corresponds to 2 atomic layers of D.

For each target, E_s=4.4 eV was assumed down to 10 A depth, while E_d=20 eV was assumed elsewhere. The Model 1 binding energy, i. e., $E_b=E_d$, was used everywhere in the target.

The calculations were made by two codes, named SP and PR codes./5/ Both codes are basically the same except that the PR code traces merely the primary particles and no trace is made for recoiled atoms to save computing time. The PR code was used to estimate the projected range and the reflection rate of the projectile. The SP code traces all of the moving particles in the cascade. Obviously the SP code consumes much longer computing time than the PR code to trace each history of the primary particle.

An example of calculated projected range distributions is shown in Fig. 5. The data are for the case of 10 keV D^+ ion injection into the NiD–mixture target, and are in comparison with the corresponding ones of the pure Ni metal. The projected range of D^+ is clearly reduced by the existence of D atoms among the Ni atoms. The slowing down of D^+ ion proceeds more quickly in the NiD target by means of D–D collisions.

Table IV summarizes the calculated results of the averaged projected range and the width of the range distribution for the four metals, where the width of the distribution is expressed by one standard deviation of D^+ stopping depth from the mean depth.

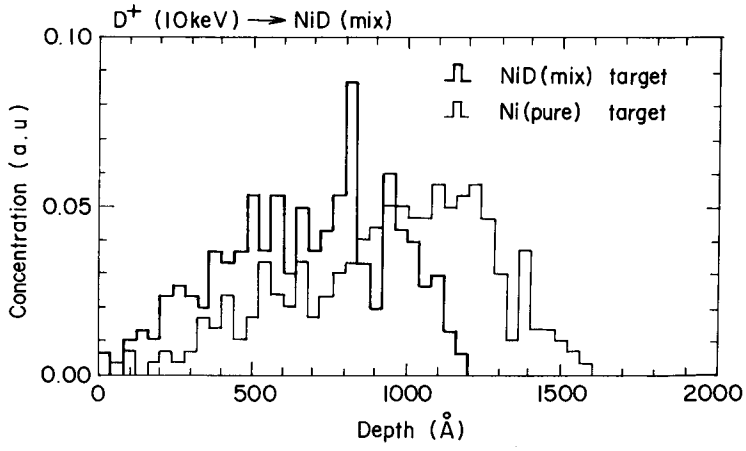

Fig. 5 Projected range distributions of 10-keV D^+ implanted into NiD (mixture) and pure Ni targets.

Table IV Averaged Projected Range and the Width of the Range Distribution (One Standard Deviation) of D^+ Ions in Ni, NiO, NiD(Mixture) and Ni with D Absorbate.

D^+ Energy (keV)	D^+ Projected Range (Width of Range Distribution) (Å) (Å)			
	Ni	NiO	NiD(mix)	D(5Å)+Ni
0.1	26.7 (15.0)	22.2 (13.4)	16.7 (9.3)	27.4 (17.4)
1	116.3 (58.9)	112.4 (59.0)	90.0 (48.5)	116.9 (66.9)
10	945.2 (316.1)	818.7 (314.4)	674.7 (269.2)	905.9 (332.1)

The slowing down effect of D^+ ions by elastic collisions becomes more pronounced as the mass number of target atoms becomes smaller. The smallest D^+ stopping depth is seen in the NiD (mixture) among the tested cases. Then the depth increases for NiO and then for Ni. The range in the Ni with D adsorbate layer agrees with the range in the pure Ni within statistical error, not being affected by the D layer at the surface.

Figures 6 and 7 illustrate the depth distribution of the displacement rate of Ni and D atoms, respectively, in the NiD mixture induced by 1 keV D^+ ions. The Ni displacement rate data in the NiD (mixture) are compared with the data in the pure Ni. The existence of D atoms decreases both the displacement rate of Ni atoms and the averaged depth of the distribution.

The displacement rate of D atoms is much larger in absolute value than the Ni atom displacement. Cascade displacement is induced among D atoms, while cascade displacement

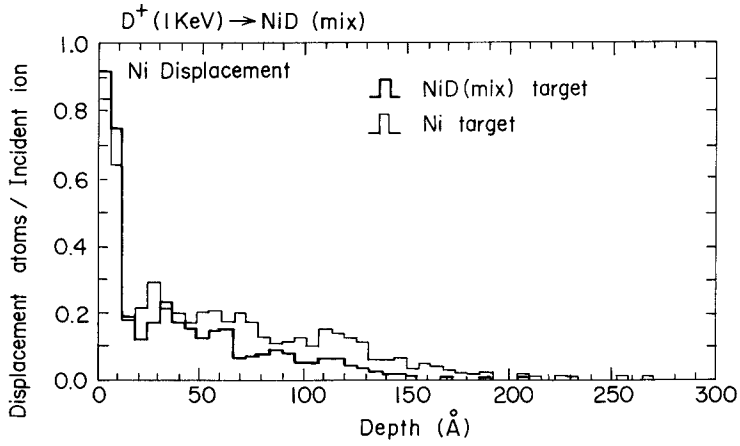

Fig. 6 Depth distributions of displacement rate of Ni atoms in NiD (mixture) and Ni targets induced by 1-keV D^+ implantation.

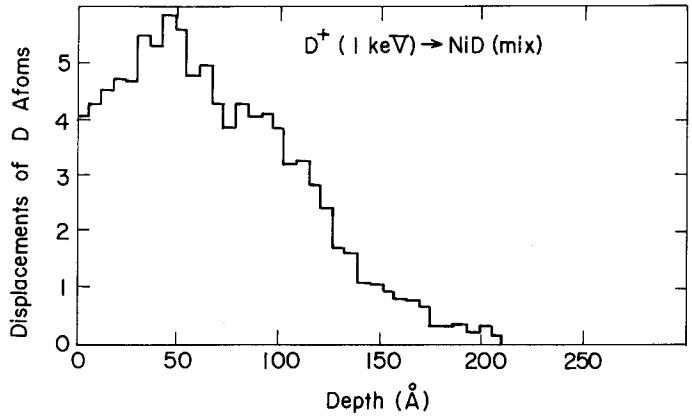

Fig. 7 Depth distribution of displacement rate of D atoms in NiD (mixture) target induced by 1-keV D^+ implantation.

Table V Number of Displacement Events of Target Atoms Induced by D^+ Ion Injection into Ni, NiO, NiD(Mixture) and Ni with D absorbate.

D^+ Energy (keV)	Displacement (1/D^+ Ion)						
	Ni	NiO		NiD(Mix)		D(5Å)+Ni	
	Ni	Ni	O	Ni	D	Ni	D
0.1	0.94	0.59	1.2	0.7	16.8	0.48	5.5
1	4.8	2.4	3.2	3.9	100.3	3.7	3.4
10	20.7	11.6	9.7	18.1	456.8	19.8	1.4

is not evident for Ni atoms. This is seen in the profile of the D-atom displacement, where a peak is observed at 50-Å depth. The number of displaced D atoms becomes the largest at this depth, as the cascade of D atoms grows with the depth and then diminishes gradually from this depth.

Table V summarizes the calculated results of the displacement rate in each target. Oxygen atoms in the NiO target decrease the Ni displacement. However, the total amount of the displacement in the target including O atoms is about the same as in the Ni metal. In the NiD (mixture) target, the Ni displacement is reduced to about 80–90% of the value of the Ni target. Although the number of the D displacement is very large, the absorption of D atoms causes only a moderate effect on the Ni displacement.

The number of total displacement events per unit incident ion energy decreases as the ion energy increases. This is due to increasing dispersion of the energy by the inelastic energy loss process in higher energy collisions.

Table VI Reflection of D^+ Ions and Emission of D in Target Induced by the Injection of D^+ Ions onto Ni, NiO, NiD(Mixture) and Ni with D absorbate layer.

D^+ Energy (keV)	Reflection and Emission Rates of D (1/D^+ Ion)					
	Ni	NiO	NiD(Mix)		D(5Å)+Ni	
				D in Target		D in Target
0.1	0.49	0.39	0.32	0.14	0.46	0.14
1	0.28	0.13	0.19	0.03	0.26	0.06
10	0.013	0.03	0.043	0.0	0.017	0.0

Table VI lists the calculated results for the reflection rate of incident D^+ ions. The emission rate of D which is originally contained in the metals is shown separately. In general, the reflection rate decreases with the ion energy, since the ion of higher energy goes deeper into the metal. Also the reflection rate decreses with a decrease in the mass of target atoms, since a larger number of projectiles tend to be scattered in the forward direction by a target atom of smaller mass. So the reflection rate is smallest for NiD, moderate for, NiO and highest for Ni. The Ni with a D absorbate layer exhibits a similar reflection rate as does the pure Ni. This means the existence of the D-atom layer in front of the Ni had only a minor effect on the reflection of the primary D^+ ion. However, adding D atoms ejected from the metal, the Ni with a D adsorbate layer emitted the largest number of D atoms in the tested cases in response to the D^+ injection.

IV Conclusions

(1) The change in the binding energy of atoms affected the displacement rate by 20% at maximum, depending on the ion energy and the mass number.

(2) The sputtering yield of Ni induced by Ar^+ and Ni^+ ions was well reproduced by the calculation except at higher energies.

(3) The D^+projected range was predicted at a slightly smaller value than the experimental result.

(4) The NiD mixture showed the most drastic change in the D^+ projected range and in the Ni atom displacement among the tested cases as compared to the pure Ni metal.

(5) The displacement rate of D atoms in the NiD (mixture) was very large.

(6) The amount of the reemission of D, including both the reflection of primary D ions and the emission of absorbed D atoms, was the largest for the Ni with D adsorbate.

References

1) J. R. Beeler, Jr., "Computer Experiments to Predict Radiation Effects in Reactor Materials," IAEA-SM-120/E-1 in "Radiation Damage in Reactor Materials, Vol. II," IAEA (1969).
2) M. T. Robinson and I. M. Torrens, Phys. Rev., 99, 1287 (1955).
3) J. P. Biersack and L. G. Haggmark, Nucl. Instr. Methods, 174, 257 (1980).
4) Y. Yamamura, Nucl. Instr. Methods in Phys. Res., B33, 429 (1988).
5) Y. Kido and T. Koshikawa, J. Appl. Phys., 67, 187 (1990).
6) G. Moliele, Z. Naturforsch, 2A, 133 (1947).
7) W. D. Wilson and C. L. Bisson, Phys. Rev., 133, 3984 (1971) ; W. D. Wilson, L. G. Haggmark and J. P. Biersack, Phys. Rev. B15, 2458 (1977).
8) D. B. Firsov, Zhur. Eksper. Teor. Fiz., 33, 696 (1957), I. Engle Transl., Sov. Phys. -JETP6, 534 (1958).
9) H. H. Anderson and J. F. Ziegler, "Hydrogen Stopping Powers and Ranges in All Elements," Pergamon Press, New York 1977.
10) J. F. Ziergler, "Helium Stopping Powers and Ranges in All Elemental Matter," Pergamon Press, New York 1977.
11) J. Lindhard and M. Scharff, Phys. Rev., 124, 128 (1961).
12) H. A. Bethe, Ann. Phys., 5, 325 (1930) ; F. Block, Ann. Phys., 16, 285 (1033).
13) C. Varelas and J. P. Biersack, Nucl. Instr. Methods, 79, 213 (1979).
14) N. Matsunami et al., Nucl. Data and Atomic Data Tables, Vol. 31, No. 1 (1983).